Monthly Notices
of the
ROYAL ASTRONOMICAL SOCIETY

MNRAS **432,** 2945–2961 (2013) doi:10.1093/mnras/stt653
Advance Access publication 2013 May 11

Calibration errors unleashed: effects on cosmological parameters and requirements for large-scale structure surveys

Dragan Huterer,[1]⋆ Carlos E. Cunha[1,2] and Wenjuan Fang[1,3]

[1]*Department of Physics, University of Michigan, 450 Church St, Ann Arbor, MI 48109-1040, USA*
[2]*Kavli Institute for Particle Astrophysics and Cosmology, 452 Lomita Mall, Stanford University, Stanford, CA 94305, USA*
[3]*Department of Astronomy, University of Illinois at Urbana-Champaign, Urbana, IL 61801, USA*

Accepted 2013 April 15. Received 2013 April 12; in original form 2012 November 26

ABSTRACT

Imperfect photometric calibration of galaxy surveys due to either astrophysical or instrumental effects leads to biases in measuring galaxy clustering and in the resulting cosmological parameter measurements. More interestingly (and disturbingly), the spatially varying calibration also generically leads to violations of statistical isotropy of the galaxy clustering signal. Here we develop, for the first time, a formalism to propagate the effects of photometric calibration variations with arbitrary spatial dependence across the sky to the observed power spectra and to the cosmological parameter constraints. We develop an end-to-end pipeline to study the effects of calibration, and illustrate our results using specific examples including Galactic dust extinction and survey-dependent magnitude limits as a function of zenith angle of the telescope. We establish requirements on the control of calibration so that it does not significantly bias constraints on dark energy and primordial non-Gaussianity. Two principal findings are (1) largest-angle photometric calibration variations (dipole, quadrupole and a few more modes, though not the monopole) are the most damaging and (2) calibration will need to be understood at the ~ 0.1 per cent–1 per cent level (i.e. rms variations mapped out to accuracy between 0.001 and 0.01 mag), though the precise requirement strongly depends on the faint-end slope of the luminosity function and the redshift distribution of galaxies in the survey.

Key words: large-scale structure of Universe.

1 INTRODUCTION

Large-scale structure (LSS) measurements have become an extremely powerful probe of cosmology over the past 30 years. Starting with the pioneering Harvard-CfA survey (de Lapparent, Geller & Huchra 1986), all the way to the Sloan Digital Sky Survey (SDSS; York et al. 2000) and its extension Baryon Oscillation Sky Survey (Dawson et al. 2013), Two-degree Field survey (Colless et al. 2001), and WiggleZ (Drinkwater et al. 2010), the LSS surveys have revolutionized our understanding of the distribution of matter and energy in the cosmos, and helped impose percent-level constraints on the cosmological parameters (e.g. Anderson et al. 2013).

A major challenge in current and future imaging and spectroscopic LSS surveys is understanding the sample selection. We define calibration to be the measure of our understanding of the selection of our sample of galaxies, and calibration errors to be any unaccounted-for angular and redshift variations in the selection. The purpose of this paper is to determine how well calibration errors need to be controlled in order to avoid substantial degradation of the information we can extract from the LSS.

A particular source of uncertainty is known as *photometric calibration*. The term refers to the adjustments required to establish a consistent spatial and temporal measurement of flux of the target objects in the different bands of observation throughout the entire photometric survey. This is an enormous problem that all existing and upcoming wide area surveys face. The difficulty comes from the variability of various building blocks of the observational pipeline, which makes it difficult to establish a consistent flux baseline at each band (i.e. the flux zero-points). In other words, because the instrument sensitivity is constantly changing, and so are the sources and intensity of noise, it is difficult to consistently compare the fluxes for objects at different parts of the sky imaged at different times. Some examples of the manifestations of the photometric calibration errors in surveys are as follows.

⋆ E-mail: huterer@umich.edu

• *Detector sensitivity:* at any given time, the sensitivity of the pixels on the camera vary along the focal plane. In addition, the sensitivity of a given pixel can change with time.

• *Observing conditions:* wide area surveys are carried out over several years and conditions are constantly changing. Observing conditions suffer from constant spatial and temporal variations.

• *Bright objects:* the light from foreground bright stars and galaxies affects the sky subtraction procedure, which impairs the surveys' completeness near bright objects (Aihara et al. 2011; Ross et al. 2011), and distorts the measured shapes of these faint galaxies (Mandelbaum et al. 2005).

• *Dust extinction:* dust in the Milky Way absorbs light from the distant galaxies. As we show later, imperfect extinction correction can have serious consequences to cosmological clustering analyses.

• *Star–galaxy separation:* in photometric surveys, faint stars can be erroneously included in the galaxy sample. Conversely, galaxies are sometimes misclassified as stars and culled from the sample. These effects are important because stars are not randomly distributed across the sky.

• *Deblending:* galaxy images can overlap, and it can be difficult to cleanly separate photometric and spectroscopic measurements for the blended objects.

Variabilities in the instrument sensitivity and observing conditions cause an angular variability in the depth of observations that the survey can achieve through each filter. Variations in the depth result in angular variations in the number density and redshift distribution of objects. In addition, because galaxy spectra are not flat, and because the sample selection involves more than one filter, depth variations cause variations in the angular and redshift distribution of galaxy types.

This variability in the sample selection can, in principle, be accounted for. This is not always done, however, and it is common, for example, for correlation analyses of current data to assume a constant depth for the entire survey. Indeed, several sources of variability have been accounted for in the analysis of existing data – see in particular the pioneering work on the subject in the modern era of LSS surveys by Scranton et al. (2002) (see also Vogeley 1998), and the more recent efforts by Ho et al. (2012) and Ross et al. (2011). These authors modelled a wide variety of systematic errors, some of which qualify as the calibration errors (e.g. seeing, airmass, calibration offsets). In particular, the latter two papers identified bright stars as the major contaminant which adds significant power to the intrinsic clustering signal at large scales, and they applied two separate successful techniques to subtract this systematic contamination.

For the upcoming surveys, an even more detailed analysis will be needed, ideally utilizing a formalism that is suited to a wide variety of photometric calibration systematics mentioned above and captures any kind of calibration-related systematic. One would also like to provide guidance on how much calibration error, as a function of scale, can be tolerated in order not to degrade the cosmological parameter inferences. Here, we aim to address both of these desiderata.

In this paper, we set out to study calibration errors in the most general way possible. Our goal is to build an end-to-end pipeline into which we can feed calibration errors (or uncertainties) due to an arbitrary cause, and from which we obtain biases in cosmological parameters inferred from the measurements of galaxy clustering in some LSS survey. We then turn the problem around, and estimate how well the calibration errors need to be controlled in order not to appreciably bias the cosmological parameter estimates.

To keep the scope of this paper reasonable, we only consider the measurements of the galaxy two-point correlation function (i.e. its Fourier transform, the power spectrum), and leave other observable quantities – higher order correlation functions of galaxies, for example – for future work. We also do not consider the effect of the photometric redshift errors which, while very important, are not expected to change our results in a major way, so we leave the photo-zs for a future analysis.

The paper is organized as follows. In Section 2, we describe our formalism of modelling both the true, underlying galaxy density field and the systematic errors describing variations in the photometric calibration. In Section 3, we present the formalism to derive cosmological constraints and biases on cosmological parameters. In Section 4, we propagate the effects of the systematic errors to calculate the biases in the cosmological parameters. We conclude in Section 5. Important technical details regarding various aspects of the computation of the effects of the photometric variation systematics on the observable quantities are relegated to the three Appendices.

2 FORMALISM: DESCRIBING SPATIALLY VARYING CALIBRATION

In this section, we start by defining calibration errors and their field $c(\hat{\boldsymbol{n}})$, and proceed to derive the biased galaxy fluctuations in terms of this field in multipole space.

2.1 Calibration errors: definition and basics

Let true galaxy counts on the sky be denoted by $N(\hat{\boldsymbol{n}})$, where $\hat{\boldsymbol{n}}$ is an arbitrary spatial direction. The survey mean is given by $\bar{N} \equiv \langle N(\hat{\boldsymbol{n}})\rangle_{\rm sky}$, where the average here is taken over the observed sky. These true fluctuations in the galaxy counts can be expanded into harmonic coefficients $a_{\ell m}$ as

$$\frac{N(\hat{\boldsymbol{n}}) - \bar{N}}{\bar{N}} = \sum_{\ell=0}^{\infty} \sum_{m=-\ell}^{\ell} a_{\ell m} Y_{\ell m}(\hat{\boldsymbol{n}}). \tag{1}$$

Consider a survey where a *deterministic* calibration error $c(\hat{\boldsymbol{n}})$ biases galaxy counts. In other words, given the true galaxy number counts in some direction $N(\hat{\boldsymbol{n}})$, the observed number is

$$N_{\rm obs}(\hat{\boldsymbol{n}}) = [1 + c(\hat{\boldsymbol{n}})]\, N(\hat{\boldsymbol{n}}), \tag{2}$$

which implicitly defines the calibration field $c(\hat{\boldsymbol{n}})$. We can expand the calibration field relative to its fiducial value of zero (corresponding to no error)

$$c(\hat{\boldsymbol{n}}) = \sum_{\ell_1=0}^{\ell_{\rm calib,max}} \sum_{m_1=-\ell_1}^{\ell_1} c_{\ell_1 m_1} Y_{\ell_1 m_1}(\hat{\boldsymbol{n}}), \tag{3}$$

where hereafter we assume that the calibration error dominates on large scales, and persists only out to some maximum multipole $\ell_{\rm calib,max}$, corresponding to the minimal angular scale of $\pi/\ell_{\rm calib,max}$ radians.

The statistical properties of the two galaxy number-density field, and the calibration-error field are, respectively

$$\begin{aligned} &\langle a_{\ell m}\rangle = 0; \qquad \langle a_{\ell m} a^*_{\ell' m'}\rangle = \delta_{mm'}\delta_{\ell\ell'} C_\ell \\ &\langle c_{\ell m}\rangle = c_{\ell m}; \quad \langle c_{\ell m} c^*_{\ell' m'}\rangle = c_{\ell m} c^*_{\ell' m'}. \end{aligned} \tag{4}$$

Throughout the paper, angular brackets $\langle\cdot\rangle$ indicate ensemble averages, that is, averages over different realizations of the Universe. To reiterate, $N(\hat{\boldsymbol{n}})$ is the Gaussian random, isotropic field as predicted by inflation, while $c(\hat{\boldsymbol{n}})$ is a deterministic function given by calibration errors in the survey at hand.

In the remainder of this paper, we use the following definition: calibration variations (or errors) are departures of $c(\hat{\boldsymbol{n}})$, or its harmonic coefficients $c_{\ell m}$, from zero. Our goal is to estimate how accurately those variations have to be known in order not to bias the cosmological parameter estimates.

Notice that we do not lose any generality by assuming that the c-field is fixed, rather than stochastic like the true galaxy density field. In this paper, we are effectively asking how much does this fixed systematic error bias the usual cosmological constraints. We are, of course, free to iterate over a number of specific incarnations of this 'fixed' error. A more specific example would be to ask how much does the Galactic dust pattern – its direction and amplitude fixed for the moment – bias some cosmological inference if unaccounted for perfectly, and then to repeat the analysis for a number of dust pattern realizations, or even for several different dust models.

2.2 Galaxy clustering and calibration errors: general case

We now derive the main results regarding the effect of the calibration errors on the observed clustering of galaxies. Let us first calculate the observed density contrast of galaxies:

$$\begin{aligned} \delta^{\rm obs}(\hat{\boldsymbol{n}}) \equiv \frac{N_{\rm obs} - \bar{N}_{\rm obs}}{\bar{N}_{\rm obs}} &= \left[\frac{N(1 + c(\hat{\boldsymbol{n}}))}{\bar{N}(1+\epsilon)} - 1\right] \\ &= \frac{1}{1+\epsilon}\left[\delta(\hat{\boldsymbol{n}})\,(1 + c(\hat{\boldsymbol{n}})) + c(\hat{\boldsymbol{n}}) - \epsilon\right] \\ &= \frac{1}{1+\epsilon}\left[\delta(\hat{\boldsymbol{n}})\left(1 + \sum_{\ell,m} c_{\ell m} Y_{\ell m}\right) + \sum_{\ell,m} c_{\ell m} Y_{\ell m} - \epsilon\right], \end{aligned} \tag{5}$$

where $Y_{\ell m} \equiv Y_{\ell m}(\hat{\boldsymbol{n}})$, and we expanded the photometric calibration variation field $c(\hat{\boldsymbol{n}})$ into spherical harmonics. Here, ϵ is the relative bias in the measured mean number of galaxies:

$$\bar{N}_{\rm obs} \equiv \langle N_{\rm obs}(\hat{\boldsymbol{n}})\rangle_{\rm sky} = \bar{N} + \sum_{\ell m} c_{\ell m} \langle N(\hat{\boldsymbol{n}}) Y_{\ell m}(\hat{\boldsymbol{n}})\rangle_{\rm sky} \equiv \bar{N}(1+\epsilon) \tag{6}$$

(the $\langle\rangle_{\rm sky}$ denotes sky average), so that

$$\epsilon \equiv \frac{1}{\bar{N}} \sum_{\ell m} c_{\ell m} \langle N(\hat{\boldsymbol{n}}) Y_{\ell m}(\hat{\boldsymbol{n}})\rangle_{\rm sky}. \tag{7}$$

The quantity ϵ can be evaluated directly in real space as above when given the calibration error map, or in harmonic space, combining equation (7) and equation (1)

$$\epsilon = \frac{c_{00}}{\sqrt{4\pi}} + \sum_{\ell,m} \frac{c_{\ell m} a^*_{\ell m}}{4\pi}, \tag{8}$$

where we used the identity $(-1)^m a_{\ell(-m)} = a^*_{\ell m}$ and the orthogonality relation for spherical harmonics. In cases where $f_{\rm sky} < 1$, the orthogonality relation does not hold, but equation (8) still does if the coefficients $a_{\ell m}$ are interpreted as the cut-sky harmonics of the density field.

The observed galaxy overdensity field can also be expanded in terms of the harmonic basis

$$\delta^{\rm obs}(\hat{\boldsymbol{n}}) \equiv t(\hat{\boldsymbol{n}}) = \sum_{\ell m} t_{\ell m} Y_{\ell m}(\hat{\boldsymbol{n}}), \tag{9}$$

Equating this to the last expression in equation (5) and inverting by multiplying with $Y^*_{\ell m}$ and using the orthogonality relation, we obtain the harmonic coefficients of the observed galaxy overdensity field $t_{\ell m}$ in terms the true galaxy fluctuation field $a_{\ell m}$ and the calibration field $c_{\ell m}$

$$t_{\ell m} = \frac{1}{1+\epsilon}\left[a_{\ell m} + c_{\ell m} + \sum_{\ell_1 \ell_2 m_1 m_2} R^{\ell_1 \ell_2 \ell}_{m_1 m_2 m}\, c_{\ell_1 m_1} a_{\ell_2 m_2} - \sqrt{4\pi}\epsilon\, \delta_{\ell 0}\, \delta_{m 0}\right], \tag{10}$$

where to obtain the last term in the last line we used $1 = \sqrt{4\pi} Y_{00}$. Here, we define the coupling matrix $\mathbf{R}$ in terms of Wigner 3j symbols

$$R^{\ell_1 \ell_2 \ell}_{m_1 m_2 m} \equiv (-1)^m \sqrt{\frac{(2\ell_1+1)(2\ell_2+1)(2\ell+1)}{4\pi}} \begin{pmatrix} \ell_1 & \ell_2 & \ell \\ 0 & 0 & 0 \end{pmatrix} \begin{pmatrix} \ell_1 & \ell_2 & \ell \\ m_1 & m_2 & -m \end{pmatrix}. \tag{11}$$

Calculating the two-point correlation of $t_{\ell m}$ is now straightforward, and things are simplified because all terms proportional to a single power of $a_{\ell m}$ (or its conjugate) vanish – recall that $c_{\ell m}$ are just some numbers here. Moreover, we can ignore the term proportional to $\delta_{\ell 0}$ – last term in equation (10) – since it only affects the monopole which is not used in cosmological constraints. The ensemble average of the multipole moments becomes, after some algebra

$$\langle t_{\ell m} t^*_{\ell' m'} \rangle = \frac{1}{(1+\epsilon)^2} \left\{ \underbrace{\delta_{m m'} \delta_{\ell \ell'} C_\ell}_{\text{isotropic}} + \underbrace{\left[U^{\ell' \ell}_{m' m}\, C_{\ell'} + (U^{\ell \ell'}_{m m'})^*\, C_\ell\right] + \sum_{\ell_2 m_2} U^{\ell_2 \ell}_{m_2 m} (U^{\ell_2 \ell'}_{m_2 m'})^*\, C_{\ell_2} + c_{\ell m} c^*_{\ell' m'}}_{\text{breaks statistical isotropy}} \right\}, \tag{12}$$

where we defined

$$U^{\ell_2 \ell}_{m_2 m} \equiv \sum_{\ell_1 m_1} c_{\ell_1 m_1} R^{\ell_1 \ell_2 \ell}_{m_1 m_2 m}, \tag{13}$$

which is a function that depends on the Wigner 3j symbols as well as the calibration-field coefficients $c_{\ell m}$.

Equation (12) is the key result in this paper. As the label in the equation shows, the observed galaxy density field $t(\hat{\boldsymbol{n}})$ exhibits *broken statistical isotropy*. In particular, the variance of t is no longer rotationally invariant (i.e. it depends on m), and covariance between the different ℓ modes is no longer zero. We can now utilize this formula and consider the isotropically measured power (i.e. assuming $\ell = \ell'$ and averaging over $m = m'$) and estimate how accurately any given systematic, described by the full set of $c_{\ell m}$, needs to be understood in order not to degrade the accuracy in measuring the cosmological parameters including non-Gaussianity[1].

2.3 Galaxy clustering and calibration errors: isotropic power case

We usually – essentially always, in fact! – assume that the field is isotropic, and then we use the data to calculate the correlation function, power spectrum, etc. Let us see how the assumed-isotropic angular power spectrum is biased in terms of an arbitrary contamination field.

Setting $\ell = \ell'$ and $m = m'$ in equation (12), we get

$$\langle |t_{\ell m}|^2 \rangle = \frac{1}{(1+\epsilon)^2} \left(C_\ell + 2 \left(U^{\ell \ell}_{m m}\right)^{\rm Re}\, C_\ell + \sum_{\ell_2 m_2} \left|U^{\ell_2 \ell}_{m_2 m}\right|^2\, C_{\ell_2} + |c_{\ell m}|^2 \right). \tag{14}$$

To assume statistical isotropy, we not only set $\ell = \ell'$ and $m = m'$ but further average over the $2\ell + 1$ values of m for a fixed ℓ. Then, we obtain the prediction for the angular power spectrum that one would measure *assuming* statistical isotropy even when the systematics break it:

$$T_\ell \equiv \frac{\sum_{m=-\ell}^{\ell} \langle |t_{\ell m}|^2 \rangle}{2\ell+1} = \frac{1}{(1+\epsilon)^2} \left[\left(1 + 2\,\frac{c_{00}}{\sqrt{4\pi}}\right) C_\ell + \frac{\sum_{m=-\ell}^{\ell} \left(\sum_{\ell_2 m_2} |U^{\ell_2 \ell}_{m_2 m}|^2\, C_{\ell_2} + |c_{\ell m}|^2\right)}{2\ell+1} \right], \tag{15}$$

where $|U|^2 \equiv U U^*$, and where the sum over ℓ_2 goes in principle over all multipoles (though only those from the range $[\ell - \ell_{\rm calib,max}, \ell + \ell_{\rm calib,max}]$ are non-zero), while m_2 goes from $-\ell_2$ to ℓ_2. Note that the term linear in U seen in equation (14) dramatically simplified in the expression for T_ℓ (equation 15) after we used the summation relation

$$\sum_{m=-\ell}^{\ell} (-1)^m \begin{pmatrix} \ell_1 & \ell & \ell \\ 0 & m & -m \end{pmatrix} = (-1)^\ell \sqrt{2\ell+1}\, \delta_{\ell_1 0}. \tag{16}$$

[1] One could also study how well one can utilize the full power of LSS measurements – by *not* assuming statistical isotropy (i.e. the full $\ell\ell' m m'$-dependent expression) – to detect, and potentially correct for, the systematics. We will study prospects for such 'self-calibration' – determination of the systematic errors internally from the survey, utilizing the $\ell \neq \ell'$, $m \neq m'$ correlators – in a future work.

For a pure monopole calibration error (i.e. a pure c_{00} term), one can verify that the effects of the ϵ term and the c_{00} term in equation (15) exactly cancel and T_ℓ is unchanged. This makes intuitive sense, as a shift in the monopole changes the mean counts on the sky but does not affect the density *fluctuations*.

One can intuitively understand the individual terms on the right-hand side of equation (15).

- The $(1+\epsilon)^{-2}$ pre-factor accounts for the change in the mean number of galaxies observed on the sky; see equation (6). As already mentioned, this term effectively ensures that the effect of the monopole (c_{00}, or constant change in calibration across the sky) is precisely cancelled out.
- The terms containing $U^{\ell_2\ell}_{m_2 m}$ introduce coupling between the multipoles. In particular, if there are calibration error multipoles out to some multipole $\ell_{\rm calib,max}$, then the galaxy power at multipole ℓ will be contaminated by contributions coming from the range $[\ell-\ell_{\rm calib,max}, \ell+\ell_{\rm calib,max}]$, a fact familiar from spin coupling in quantum mechanics.
- Presence of the term $|c_{\ell m}|^2$ essentially means that the power of the calibration field is added to the intrinsic galaxy power spectrum. In other words, even if the distribution of galaxies on the sky were perfectly uniform so that $\delta \equiv N/\bar{N} - 1 = 0$ over some area, the calibration field will induce power so that $\delta^{\rm obs} \neq 0$.

From the structure of equation (15), it is clear that calculating and storing the coefficients U is challenging. Naively, the problem requires evaluation of roughly 10^{18} coefficients. Appendix C describes our approach of limiting the number of evaluations of $(\ell, \ell_1, \ell_2, m, m_1, m_2)$ and tabulating the coefficients U so that the number of operations is only of the order of 10^8 (for $\ell_{\rm max} = 1000$ binned in $\sim$30 multipole bins and considering the calibration variations out to $\ell_{\rm calib,max} = 20$), and is thus feasible. We plot the biased power spectra T_ℓ further below in the next section.

Finally, it is worth writing down the observed angular *cross-correlation* power spectrum between fluctuations $t^{(i)}_{\ell m}$ and $t^{*(j)}_{\ell m}$ in two different tomographic redshift bins i and j; it follows straightforwardly from equation (15) that

$$T^{(ij)}_\ell = \frac{1}{(1+\epsilon^{(i)})(1+\epsilon^{(j)})}\left[\left(1+\frac{c^{(i)}_{00}+c^{(j)}_{00}}{\sqrt{4\pi}}\right)C^{(ij)}_\ell + \frac{\sum_m\left(\sum_{\ell_2 m_2}(U^{\ell_2\ell}_{m_2 m})^{(i)}\,(U^{\ell_2\ell}_{m_2 m})^{*(j)}\,C^{(ij)}_{\ell_2} + c^{(i)}_{\ell m}c^{*(j)}_{\ell m}\right)}{2\ell+1}\right], \tag{17}$$

where $c^{(i)}_{\ell m}$, $\epsilon^{(i)}$ and $(U^{\ell_2\ell}_{m_2 m})^{(i)}$ are all evaluated in the redshift bin i (and same for j), and where $C^{(ij)}_\ell$ are the true galaxy cross-correlation power spectra. While the physical sources of calibration error are typically local and thus redshift-independent, in Section 4, we demonstrate that converting from the magnitude error to the calibration field $c(\hat{\boldsymbol{n}}) \equiv (\delta N/N)(\hat{\boldsymbol{n}})$ depends on the faint-end slope of the luminosity function, which typically *is* redshift dependent, hence making the harmonic coefficients of $c(\hat{\boldsymbol{n}})$ also z dependent and thereby potentially introducing couplings between the different redshift bins.

2.4 Additive and multiplicative systematics

Before we obtain numerical results on how some realistic calibration errors affect the observed power spectra, it pays to consider qualitatively how the angular power spectrum of galaxies is affected.

It is often useful to divide the effect of systematic errors into *additive* (those whose field is added to the true field observed on the sky), and *multiplicative* (those whose field multiplies the true field); see Gordon et al. (2005) where his nomenclature has been previously employed in the cosmic microwave background (CMB) context, and Huterer et al. (2006) and Heymans et al. (2006) who considered the additive and multiplicative systematic errors in weak lensing measurements. These terms refer to the systematic error that either adds to the true galaxy fluctuations, or else multiplies it and modulates the true signal; see equation (5) for the real-space and equation (10) for the harmonic-space picture. For example, on the right-hand side of equation (10) the term $a_{\ell m}$ corresponds to the true density field, $c_{\ell m}$ represents the additive effect of the systematic error, while the term containing $c_{\ell m}a_{\ell m}$ term together with the geometric factor $\boldsymbol{R}$ and the appropriate sum represents the multiplicative effect of the systematics[2].

Additive and multiplicative errors in the counts translate into additive and multiplicative contributions from the calibration field to the observed galaxy power spectrum, see equation (12): the additive error is the term $c_{\ell m}c^*_{\ell m}$ while the multiplicative error are all terms involving the coupling matrix $\mathbf{U}$. The two kinds of errors produce qualitatively different effects: additive error at some multipole ℓ_1 only affects power at that multipole, while the multiplicative error affects power at a range of multipoles; in particular, true power at an arbitrary multipole ℓ would leak to all multipoles in the range $[\ell-\ell_1, \ell+\ell_1]$.

The additive terms dominate the error budget on the largest scales, but are subdominant at smaller scales (Vogeley 1998). This can be understood qualitatively as follows: modulo geometric coupling terms, both additive and multiplicative terms are proportional to the square of coefficients $c_{\ell m}$, but the multiplicative terms are further multiplied by the fiducial angular power C_ℓ. Given that $C_\ell \ll 1$ at all ℓ and any redshift[3], the multiplicative terms are suppressed relative to the additive terms. At higher multipoles, on the other hand, there are more ways in

[2] Technically speaking, the systematic effects are all multiplicative in equation (10) because of the $1/(1+\epsilon)$ pre-factor; however, given that this pre-factor is typically very close to unity, the second and third term in parentheses of this equation act approximately in the additive and multiplicative sense.

[3] One exception – C_ℓ of order unity or larger – is realized in the scenario of galaxies at a very low redshift, $z \lesssim 0.05$. However, such a sample would probably not be useful for cosmology given the significant galaxy peculiar velocities and the necessarily small volume probed. Moreover, the calibration errors would have less impact to begin with, since they would be affecting a very large intrinsic clustering signal.

which power from other scales can leak into that ℓ so that the sums associated with multiplicative terms make them the dominant systematic contribution.

While it is often assumed for simplicity that the systematic errors, calibration or other, are represented by purely additive errors, we just demonstrated that both kinds of errors are important. In fact, in the plausible scenario where largest scale information in the survey is ignored to avoid the systematic contamination, the multiplicative errors dominate. In what follows, we use the full expressions containing both additive and multiplicative terms.

3 POWER SPECTRA AND THEIR BIASES

In this section, we propagate the effect of calibration errors to estimate biases in the cosmological parameters describing dark energy and primordial non-Gaussianity.

3.1 Fiducial cosmological model

We consider a set of cosmological parameters with the following fiducial values: matter density relative to critical $\Omega_{\rm M} = 0.25$, dark energy equation of state parameter today $w_0 = -1$, its variation with scale factor $w_a = 0$, spectral index $n = 0.96$ and amplitude of the matter power spectrum $\ln A$, where $A = 2.3 \times 10^{-9}$ (corresponding to $\sigma_8 = 0.80$) defined at scale $k = 0.002\,{\rm Mpc}^{-1}$. Note that we hold fixed the Hubble constant $h = H_0/(100\,{\rm km\,s^{-1}\,Mpc^{-1}})$ (or equivalently, physical matter density $\Omega_{\rm M}h^2$), the physical baryon density $\Omega_{\rm B}h^2$, and we assumed a flat universe. On the other hand, we do not assume any other prior information, such as the CMB information from *Wilkinson Microwave Anisotropy Probe* (*WMAP*) and *Planck*. In practice, this prior information would largely serve to fix h, $\Omega_{\rm M}h^2$, $\Omega_{\rm B}h^2$, and curvature $\Omega_{\rm K}$. Note that this rather restricted the set of assumptions about the set of cosmological parameters and external information about them is sufficient for our analysis: we are primarily concerned about the effect of the calibration systematics on the measured power spectra, and on the biases in the dark energy and non-Gaussianity parameters. Given that the systematics strongly depend on the properties of the galaxy sample and the survey (as we discuss further below), it is not necessary to model the up-to-date knowledge about the cosmological parameters in great detail.

We assume a survey covering 5000 square degrees (so $f_{\rm sky} \simeq 0.12$) with information out to $z_{\rm max} = 1$, corresponding roughly to the Dark Energy Survey (DES). We assume that the number density of the galaxies is $n(z) \propto z^2 \exp(-z/z_0)$ with $z_0 = 0.3$, and that photometric redshifts enable splitting the sample in five tomographic bins centred at $z = 0.1$, 0.3, 0.5, 0.7 and 0.9; see the left-hand panel of Fig. 1. The fiducial statistical constraints on the dark energy parameters are $\sigma(w_0) = 0.06$ and $\sigma(w_a) = 0.24$.

Instead of the power spectrum in wavenumber $P(k)$, we consider measurements of the angular power spectrum of galaxy fluctuations. In the Limber approximation, which is valid on intermediate to small angular scales, the angular power is given as (e.g. Huterer, Knox & Nichol 2001; Zhan, Knox & Tyson 2009)

$$P_\ell^{(ij)} \equiv \langle a_{\ell m}^{(i)} a_{\ell m}^{*(j)} \rangle = \frac{2\pi^2}{\ell^3} \int_0^\infty r(z) H(z) b^2(k,z) \Delta^2(k,z) W_i(z) W_j(z) {\rm d}z, \tag{18}$$

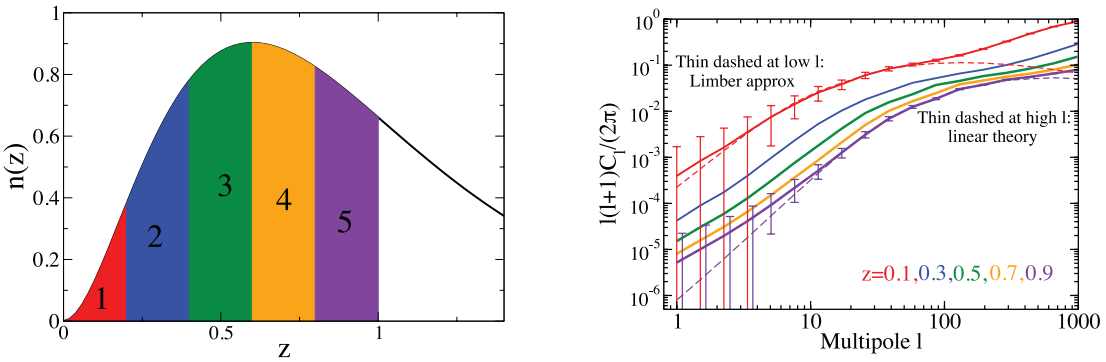

Figure 1. Left-hand panel: density distribution of galaxies assumed in this paper, and boundaries of the five redshift bins. We ignore information at $z > 1$, thus roughly modelling the difficulties with establishing accurate photometric redshifts at that range (for the DES). Right-hand panel: angular power spectra $C_\ell^{(ii)}$ for five redshift bins. (Cross-correlations between the bins, while used in the analysis, are very small and not important nor shown in the figure.) For the first and fifth bin we show, at the low-multipole end, the full expression that we use at large scales (see equation A4) and, at the high-multipole end, the linear power spectrum for reference. For the first and fifth redshift bin, we also show the cosmic variance errors plus shot noise.

where i and j are referring to one of the five redshift bins[4] and $b(k, z)$ is the bias defined below. The full, beyond-Limber expression, as well as the definition of the $W(z)$ terms, are given in Appendix A. The power spectrum $\Delta^2(k, z) \equiv k^3 P(k)/(2\pi^2)$ is calculated using the transfer function output by CAMB, and its non-linearities are modelled with the Smith, Scoccimarro & Sheth (2007) formulae that were based on a halo model and fit to simulations. Appendix A has all of the details of how we calculate the power spectrum.

We consider information from multipoles $1 \leq \ell \leq 1000$, corresponding to spatial scales from about 10 arcmin to 180 degrees. To obtain accurate constraints on the parameter $f_{\rm NL}$ which come from large angular scales, we use every individual multipole between $\ell = 1$ and $\ell_{\rm calib,max} = 20$; beyond this, we use 10 more widely separated bins with $\Delta\ell \simeq 100$. Therefore, we use a total of 30 bins in ℓ; for the low-ℓ ones, we do *not* assume the Limber approximation and use equations (A4), while for the higher multipoles, we use the Limber approximation, equation (18) above.

Finally, we also allow for the presence of primordial non-Gaussianity. We adopt the widely studied 'local' model of non-Gaussianity

$$\Phi(\boldsymbol{x}) = \Phi_{\rm G}(\boldsymbol{x}) + f_{\rm NL}\left(\Phi_{\rm G}^2 - \langle\Phi_{\rm G}^2\rangle\right), \tag{19}$$

(where Φ is the primordial Newtonian gravitational potential, $\Phi_{\rm G}$ is its Gaussian component, and $f_{\rm NL}$ is a dimensionless parameter), the bias becomes scale dependent, with a new term that goes as k^{-2} (Dalal et al. 2008)

$$b(k) = b_0 + f_{\rm NL}(b_0 - 1)\delta_c \frac{3\Omega_{\rm M}H_0^2}{a\, g(a) T(k) c^2 k^2}, \tag{20}$$

where b_0 is the usual Gaussian bias (on large scales, where it is constant), $\delta_c \approx 1.686$ is the collapse threshold, a is the scale factor, $\Omega_{\rm M}$ is the matter density relative to critical, H_0 is the Hubble constant, k is the wavenumber, $T(k)$ is the transfer function, $g(a)$ is the growth suppression factor, and c is the speed of light[5]. We assume the fiducial model with the Gaussian bias $b_0 = 2$ and zero non-Gaussianity, $f_{\rm NL} = 0$.

The full set of cosmological parameters that we use is therefore

$$p_a \in \{\Omega_{\rm M}, w_0, w_a, n, A, f_{\rm NL}\}. \tag{21}$$

The cosmological constraints can then be computed from the Fisher matrix

$$F_{ab} = \sum_{\ell,\alpha,\beta} \frac{\partial C_\ell^{(\alpha)}}{\partial p_a} {\rm Cov}^{-1}\left[C_\ell^{(\alpha)}, C_\ell^{(\beta)}\right] \frac{\partial C_\ell^{(\beta)}}{\partial p_b}, \tag{22}$$

where α and β stand for all pairs of bin indices (i, j) with $i \leq j$ (since $C_\ell^{(ji)} \equiv C_\ell^{(ij)}$). The observed power spectrum is equal to the raw power plus shot noise

$$C_\ell^{(ij)} = P_\ell^{(ij)} + \delta_{ij}\frac{1}{N_i^{\rm sr}}, \tag{23}$$

where $N_i^{\rm sr}$ is the number of galaxies per steradian in the tomographic bin i. Moreover, ${\rm Cov}^{-1}$ in equation (22) is the inverse of the covariance matrix between the observed power spectra; assuming observations in the linear (and therefore Gaussian) regime only, the covariance matrix follows directly from Wick's theorem:

$${\rm Cov}\left[C_\ell^{(ij)}, C_{\ell'}^{(kl)}\right] = \frac{\delta_{\ell\ell'}}{(2\ell+1) f_{\rm sky}\Delta\ell}\left[C_\ell^{(ik)}C_\ell^{(jl)} + C_\ell^{(il)}C_\ell^{(jk)}\right]. \tag{24}$$

The minimal error in the ith cosmological parameter is, by the Cramér–Rao inequality, $\sigma(p_i) \simeq \sqrt{(F^{-1})_{ii}}$.

Finally, we would like to estimate the bias in the cosmological parameters, δp_a, given an arbitrary systematic error in the power spectrum, δC_ℓ. The bias can be estimated using the Fisher matrix formalism as follows:

$$\delta p_a = \sum_b F_{ab}^{-1} \sum_{\ell,\alpha,\beta} \delta C_\ell^{(\alpha)} {\rm Cov}^{-1}\left[C_\ell^{(\alpha)}, C_\ell^{(\beta)}\right] \frac{\partial C_\ell^{(\beta)}}{\partial p_b}. \tag{25}$$

[4] While we use all of the cross-correlations, $i \gtrsim j$, we notice that the cosmological constraints – and requirements on the systematics – remain unchanged if we only use the angular power spectrum auto-correlations with $i = j$. This is not too surprising, as cross-correlations $C_\ell^{(ij)}$ are guaranteed to be zero in the Limber approximation and in the absence of photometric redshift errors (photo-zs generically lead to the overlap of redshift bins and thus bin-to-bin correlations). At large scales, where we do not employ the Limber approximation because it is not accurate there (especially for non-zero $f_{\rm NL}$ which introduces very large scale correlations), we explicitly verify that cross-powers do not appreciably alter our requirements on the control of the calibration errors.

[5] This formula has higher order corrections calibrated to N-body simulations and also derivable from theory, but these are typically small and not crucial for the present analysis so we ignore them here.

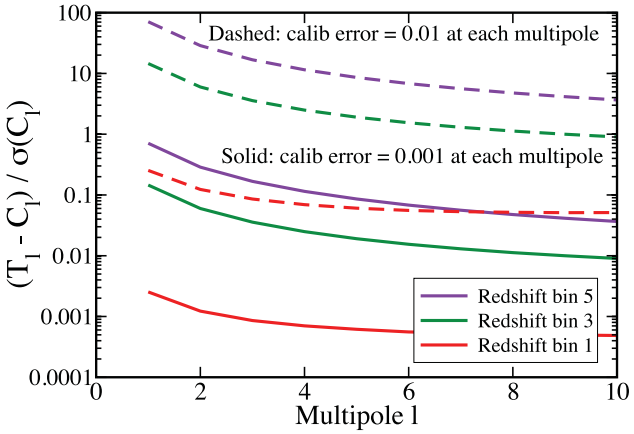

Figure 2. Difference between the observed isotropic part of the power spectrum T_ℓ (see equation 15) and the fiducial C_ℓ, divided by the statistical error (cosmic variance plus shot noise) for our assumed DES-type survey with $f_{\rm sky} \simeq 1/8$. We assume a constant rms photometric variation of 0.01 (dashed curves) or 0.001 (solid curves) per each multipole ℓ. Note that higher redshift bins are affected more than the lower redshifts. The fall-off with ℓ can be understood analytically; see the text for details.

3.2 Biases in the observed power spectra

We would like to fairly compare the biases as a function of ℓ_1, so we choose to adopt coefficients describing the uncertainties in the calibration field $c_{\ell_1 m_1}$ that lead to a *fixed variance* in the calibration pattern on the sky $c(\hat{\boldsymbol{n}})$ (and corresponding to, as we will shortly see, fixed variance in the angular variations of the magnitude limits of the survey). Thus, we have

$$\mathrm{Var}(\mathrm{c}(\hat{\boldsymbol{n}})) = \frac{2\ell_1+1}{4\pi}\mathcal{C}^{\rm sys}_{\ell_1} = \frac{|\mathrm{c}_{\ell_1 \mathrm{m}_1}|^2}{4\pi} \quad \text{(no sum)} \tag{26}$$

since $\mathcal{C}^{\rm sys}_{\ell_1} = |c_{\ell_1 m_1}|^2/(2\ell_1+1)$ is the angular power spectrum of the systematics (and really just the sum of their coefficients squared) and where the reader is reminded that, in this particular calculation we are 'turning on' one (ℓ_1, m_1) pair at a time.

To consider the calibration variation in a single multipole (ℓ_1, m_1) that leads to a fixed variance in $c(\hat{\boldsymbol{n}})$, we therefore make the choice

$$c^{\rm Re,Im}_{\ell_1 m_1} = \begin{cases} \sqrt{4\pi \mathrm{Var}(\mathrm{c}(\hat{\boldsymbol{n}}))} & (m=0) \\ \sqrt{2\pi \mathrm{Var}(\mathrm{c}(\hat{\boldsymbol{n}}))} & (m\neq 0) \end{cases}, \tag{27}$$

where in the $m \neq 0$ case both real and imaginary part of the $c_{\ell_1 m_1}$ have the given value.

Fig. 2 shows the difference between the observed isotropic part of the power spectrum T_ℓ (see equation 15) and the fiducial C_ℓ, divided by the statistical error (cosmic variance plus shot noise) for our assumed DES-type survey with $f_{\rm sky} \simeq 1/8$. We assume a constant calibration error with rms[6] of 0.01 or 0.001 per each multipole ℓ_1 separately. While a fixed ℓ_1 of the systematic errors affects all multipoles ℓ, it affects $\ell = \ell_1$ the most, so in this graph we only plot the effect on the observed power spectrum at the *same multipole* at which the systematic errors occurs. In other words, Fig. 2 shows the maximally affected multipole ℓ, for a fixed calibration variation error. The error in the measured tomographic angular power spectra decreases with multipole ℓ, which can be understood easily as follows: to a good approximation, the additional terms in the observed isotropic power spectrum, equation (15), are dominated by the additive term $|c_{\ell m}|^2/(2\ell+1)$. We find this is the case even for the lowest redshift tomographic bin, where C_ℓ is the highest and thus helps boost the multiplicative terms that contain the U coefficients. Moreover, generally we find that $\epsilon \simeq 0$. Therefore,

$$\frac{T_\ell - C_\ell}{\sigma(C_\ell)} \simeq \frac{\dfrac{|c_{\ell m}|^2}{(2\ell+1)}}{\sqrt{\dfrac{2}{(2\ell+1)f_{\rm sky}}}\left(C_\ell + \dfrac{1}{N^{\rm sr}}\right)}, \tag{28}$$

where $C_\ell \equiv C^{(ii)}_\ell$ refers to the power spectrum in some redshift bin i, and the same for T_ℓ and $c_{\ell m}$. For a fixed variance in the photometric variations, $c_{\ell m}$ is independent of ℓ, so that this expression goes as $1/[\sqrt{2\ell+1}C_\ell]$, decreasing with ℓ approximately as $\ell^{-1.3}$, at least out to $\ell = 10$ plotted in this figure.

Fig. 2 further shows that higher redshift bins are affected more than the lower redshifts. This is easy to understand: at higher redshift, the cosmological signal is smaller, given that it averages over more LSS along the line of sight, and therefore it is more susceptible to the (redshift-independent) calibration bias.

[6] For the purposes of making Fig. 2 we put all of the photometric calibration variation in a single value of $m_1 = 0$.

The one important thing to take away from Fig. 2 is therefore that the calibration error is expected to be most damaging to the deepest surveys (or highest redshift slices of a survey). And it is precisely those highest redshifts that are most valuable in providing information about dark energy and primordial non-Gaussianity.

4 SENSITIVITY TO CALIBRATION ERRORS

Let us now consider a few specific examples. First, we will study the sensitivities to an arbitrary systematic bias in calibration at each multipole *separately*, i.e. one (ℓ_1, m_1) pair at a time in the $c_{\ell_1 m_1}$. Then, we study two concrete examples of physical effects that cause calibration biases: corrections to the dust extinction maps, and variable survey depth.

4.1 From calibration to galaxy counts

Consider the observed angular density of galaxies in some direction in the sky $N(\hat{\boldsymbol{n}}) \equiv \int n(z, \hat{\boldsymbol{n}}) \mathrm{d}z$, where $n(z, \hat{\boldsymbol{n}})$ is the galaxy density in that direction and at redshift z. Calibration errors correspond to variations in the magnitude limit of the survey $\delta m_{\rm max}(\hat{\boldsymbol{n}})$. The observed density of galaxies changes since the galaxy density is a strong function of the survey depth (i.e. the magnitude limit). Suppressing the direction label $\hat{\boldsymbol{n}}$, we have

$$\delta[\log_{10} N(z, > m)] = \left.\frac{\mathrm{d}\log_{10} N(z, > m)}{\mathrm{d}m}\right|_{m_{\rm max}} \delta m_{\rm max} \equiv s(z)\delta m_{\rm max}, \tag{29}$$

where $m_{\rm max}$ is the maximal apparent magnitude observed in that direction in some waveband. It follows that the systematic bias in the observed fluctuations is

$$\left(\frac{\delta N}{N}\right)_{\rm sys} = \ln(10) s(z)\, \delta m_{\rm max}. \tag{30}$$

Often we have information about the selective extinction $E(B-V)$; the relation to magnitude extinction is $\delta m \equiv \delta A = \delta[R\, E(B-V)]$ where R is the ratio of total to selective extinction and A is the alternative notation sometimes used for extinction. Assuming that R is known perfectly[7], $\delta m \simeq R\, \delta(E(B-V))$, and thus (restoring the direction $\hat{\boldsymbol{n}}$ explicitly)

$$\left(\frac{\delta N}{N}\right)_{\rm sys}(\hat{\boldsymbol{n}}) \equiv c(\hat{\boldsymbol{n}}) = \ln(10) s(z) \delta m_{\rm max}(\hat{\boldsymbol{n}}) = \ln(10) s(z) R\, \delta(E(B-V))(\hat{\boldsymbol{n}}). \tag{31}$$

While $s(z)$ is galaxy-population dependent, we can still estimate $(\delta N/N)_{\rm sys}$ to be *very* roughly of the order of $\delta(E(B-V))(\hat{\boldsymbol{n}})$, given that $s(z)$ is of the order of 0.1–1 while R takes values between about 1 and 5 depending on the band; see e.g. the appendix of Schlegel, Finkbeiner & Davis (1998) and important updates given in the table 6 of Schlafly & Finkbeiner (2011).

4.2 Calibration Bias per Multipole

Let us consider biases in our six cosmological parameters as a function of bias in a single multipole $c_{\ell_1 m_1}$. Following the prescription in the previous section, we assume that the variance of the calibration field is fixed and constant separately at each multipole ℓ_1; see equation (27).

We now propagate the calibration variation in a given (ℓ_1, m_1), separately for $1 \le \ell_1 \le 20$ and $-\ell_1 \le m_1 \le \ell_1$, and for magnitude given in the above equations, to the observed angular power spectra via equation (15).

Fig. 3 shows the bias divided by the statistical error in cosmological parameters for the fixed *magnitude* rms variation per multipole of $\langle \delta m^2_{\rm max} \rangle^{1/2}_{\rm sky} = 0.01$ or 0.001. We use equation (31) to translate this to the calibration-field variation, and then a modified version of equation (27) to calculate the harmonic coefficients $c_{\ell_1 m_1}$ that enter the calculation:

$$c^{\rm Re,Im}_{\ell_1 m_1} = \begin{cases} \sqrt{4\pi \mathrm{Var}(\mathrm{c}(\hat{\boldsymbol{n}}))/(2\ell_1+1)} & (m=0) \\ \\ \sqrt{2\pi \mathrm{Var}(\mathrm{c}(\hat{\boldsymbol{n}}))/(2\ell_1+1)} & (m \neq 0), \end{cases} \tag{32}$$

where relative to equation (27), we have an additional term of $(2\ell_1+1)^{-1/2}$ to keep the variance in each ℓ_1 fixed since we are now distributing power over *all* m_1-modes. We adopt the fiducial redshift-dependent faint-end slope of the luminosity function, $s(z) \equiv \left.\mathrm{d}\log_{10} N(z, > m)/\mathrm{d}m\right|_{m_{\rm max}}$,

$$s(z) = 0.094 + 0.155z + 0.165z^2, \tag{33}$$

estimated from the simulations of Jouvel et al. (2009), assuming a DES i-band magnitude limit of 24. This functional form roughly describes the trend that the highest redshifts are most affected by variations in the survey depth. We emphasize that this form for $s(z)$ is meant purely for illustration, as different galaxy samples will have different $s(z)$. We consider biases in the non-Gaussianity parameter $f_{\rm NL}$, the (constant)

[7] If R is not perfectly known, as is often the case, then the magnitude variation is equal to the variation in the product between R and $E(B-V)$.

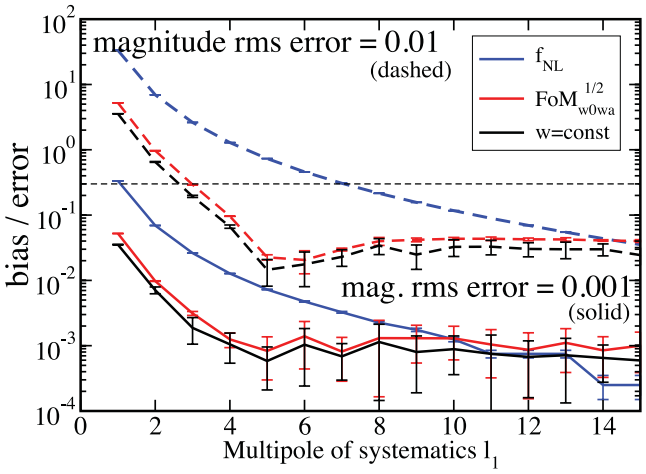

Figure 3. Bias divided by marginalized statistical error in the cosmological parameters for the fixed magnitude root-mean-squared variation of 0.001 (solid curves) or 0.01 (dashed curves), as a function of multipole at which the systematics are introduced. We show the bias/error ratio for the non-Gaussianity parameter $f_{\rm NL}$, constant equation of state of dark energy w and the square root of the DETF figure of merit, FoM$^{1/2}$, which serves to gauge any additional dependence brought forth by the temporal variation in the equation of state w_a. To convert the magnitude variation to the $\delta N/N$ error, we used equation (30) and the best-fitting faint-end slope of the luminosity function, $s(z)$, estimated from the simulations of Jouvel et al. (2009); see the text for details. The error bars show dependence on which of the m_1-values, for a fixed ℓ_1, contains the calibration error; this dependence is small at the largest scales where the calibration error clearly has the largest effect. As discussed in the text, the monopole $\ell_1 = 0$ has no effect on the biases by definition. The dashed horizontal line denotes a fixed bias/error ratio of 0.3, which is approximately the upper limit of how much effect a systematic error should have on the cosmological parameters without seriously affecting the overall constraints in a survey.

equation of state of dark energy w, and the square root of the dark energy figure-of-merit (FoM), which is the inverse area of the 95 per cent contour in the w_0–w_a plane (Huterer & Turner 2001; Albrecht et al. 2006). Note that the latter quantity takes into account the temporal variation of DE, and the square root serves to compare it fairly to the bias in constant w; the two quantities, $\sigma(w)$ and FoM$^{1/2}$, show very similar behaviour in these results. The error bar at each ℓ_1 shows the rms dispersion of the $(2\ell_1 + 1)$ values of m_1 into which we put the systematics. So, for example, at $\ell_1 = 6$ and for either one of the rms values for the calibration error, the error bars show the dispersion in the bias/error ratios for 13 different values of m_1.

Fig. 3 clearly indicates that systematic errors have the largest impact at largest angular scales assuming a fixed contribution to the variance from each multipole. Bias in the non-Gaussianity parameter $f_{\rm NL}$ is larger than that for the dark energy parameters, which is expected because most of the information on $f_{\rm NL}$ comes from large angular scales which are particularly susceptible to calibration errors. For the calibration systematics at smaller scales – ℓ_1 beyond six or so corresponding to variation at scales less than about 30° on the sky – the effect of the systematics asymptotes to a smaller value. The minimum in the FoM$^{1/2}$ and w curves around $\ell_1 \simeq 6$ is due to the transition from the dominance of the additive errors at larger scales to multiplicative errors at smaller scales. Since calibration errors at large angular scales are the most damaging, it is sufficient to consider only those, and our choice of the maximum multipole of where the error enters, $\ell_1 \leq \ell_{\rm calib,max} = 20$ is therefore sufficient.

Fig. 4 is similar to Fig. 3 except now we show the effects when the magnitude error is split equally among all multipoles less than or equal to $\ell_{1,\rm max}$ (instead of all of it being lumped in a single multipole as in Fig. 3). Given that the effect of the systematic error decreases with ℓ_1, the biases in the cosmological parameters are larger than in the previous figure. Qualitatively, the two figures paint a consistent picture of the potentially deleterious effects of the calibration variations even at a level corresponding to $O(0.001$–$0.01)$ mag.

4.3 Example I: corrections to dust maps

We now study a specific scenario of calibration systematics: corrections to the Schlegel-Finkbeiner-Davis (SFD; Schlegel et al. 1998) dust extinction maps. Dust in our Galaxy causes extinction, which in turn alters the observed galaxy fluctuations across the sky. While the Galactic dust has been mapped out reasonably accurately, we ask how accurately it *needs to* be mapped out in order not to bias the cosmological parameters.

To start, we need a model for the variations in the SFD map. We adopt results from the work of Peek & Graves (2010) (hereafter PG10) who used 'standard crayons' – objects of known colour – in the SDSS to correct the SFD maps over the north galactic cap region (for a related work, see Schlafly & Finkbeiner 2011). Schematically, therefore

calibration variations ≡ (PG10–SFD).

The SFD map is shown in the top-left panel of Fig 5, while the PG10 *correction* is displayed in the top-right panel. To convert this $E(B - V)$ map to $\delta N/N$ fluctuations (see equation 31), we assume DES observations in the i band, for which $R = 1.595$ (Schlafly & Finkbeiner 2011).

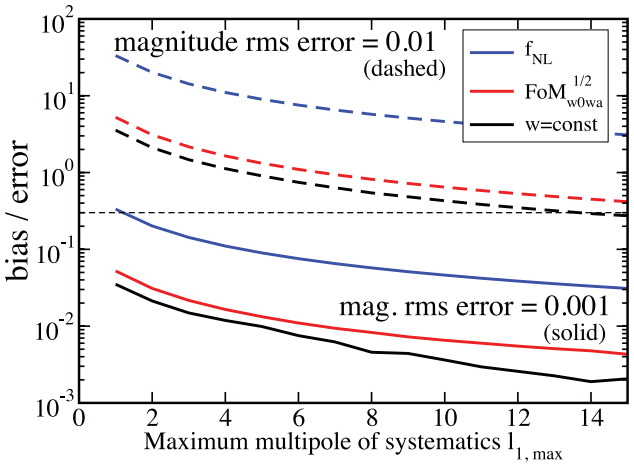

Figure 4. Same as Fig. 3, except now the fixed magnitude error of 0.001 is *shared* equally among all multipoles in the range $1 \leq \ell_1 \leq \ell_{1,\max}$. This is perhaps a more realistic assumption than the one shown in Fig. 3, where all of the error comes from a single multipole. The biases now appear larger because the contributions from the largest scales dominate the budget at a fixed $\ell_{1,\max}$.

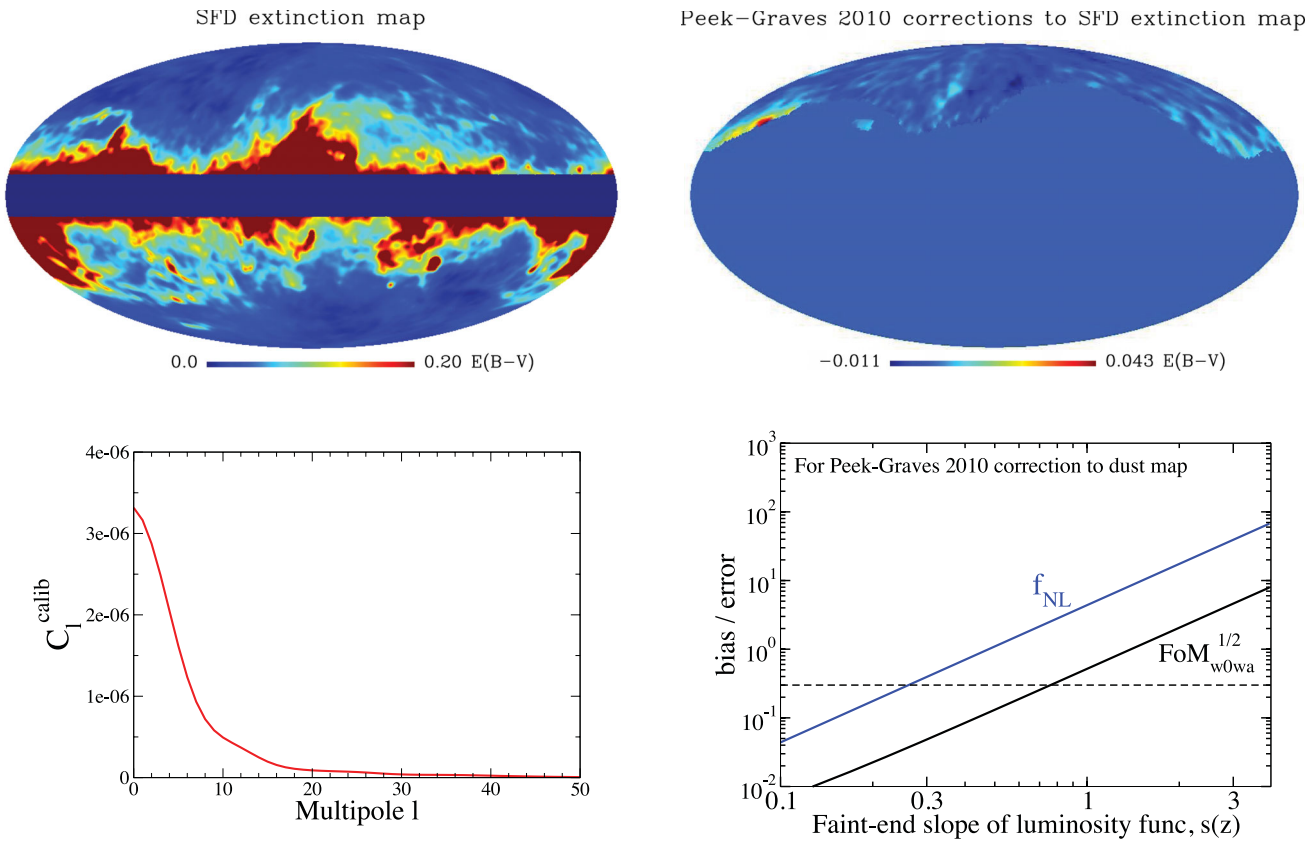

Figure 5. Top left: Schlegel et al. (1998) SFD extinction map, $E(B-V)(\hat{\boldsymbol{n}})$, in Galactic coordinates with the 10° Galactic plane cut. Top right: corrections to the SFD map from the work of Peek & Graves (2010). Bottom left: angular power spectrum of the PG10 map extracted by POLSPICE and shown without the usual $\ell(\ell+1)/(2\pi)$ term so that the relative contribution of different multipoles can be more easily seen. Bottom right: bias/error ratios for $f_{\rm NL}$ and the square root of the DETF FoM assuming PG10 map represents the calibration error, as a function of the faint-end slope of the luminosity function s. Note that the biases increase very sharply with s, roughly scaling as s^2. The desired bias/error limit (horizontal dashed line) is exceeded already for $s \simeq 0.3$ for $f_{\rm NL}$ and $s \simeq 0.8$ for the dark energy equation of state.

The bottom-left panel in Fig. 5 shows the angular power spectrum extracted using POLSPICE software package (Chon et al. 2004). As explained in Appendix B at length, the most reliable way of modelling the calibration errors was to first extract the power from the map, then generate a full-sky realization *consistent* with that power (using the `isynfast` routine in HEALPIX). We explicitly verified the intuitive expectation that the results do not depend much on the realization.

The bottom right of Fig. 5 shows the resulting biases in $f_{\rm NL}$ and the square root of the dark energy FoM, as a function of the faint-end slope of the luminosity function $s(z)$; the $w = $ const case is not shown here or in the following figure since it gives very similar results as the FoM$^{1/2}$. We assume that calibration variations are given by the PG10 corrections, and that $s(z)$ is constant in redshift (we nevertheless allow for the redshift-dependent $s(z)$ in all equations). As mentioned around equation (30), the biases are very sensitive to $s(z)$, scaling very nearly as $s(z)^2$. This can be easily understood: in Section 2.3, we mentioned that the bias in the power spectrum is dominated by the added calibration power $\propto |c_{\ell m}|^2$, while the (real-space) calibration field is linear in $s(z)$ (equation 31); hence

$$\delta p_a \propto \delta C_\ell \propto |c_{\ell m}|^2 \propto s(z)^2. \tag{34}$$

In other words, in the case where the additive calibration errors dominate so that calibration simply adds power ($|c_{\ell m}|^2$ term), the biases in the cosmological parameters are proportional to this added power, and hence to the square of the faint-end slope of the luminosity function. Therefore, the faint-end slope of the luminosity function is a key factor relating the photometric magnitude variations to the cosmological parameter biases. Steep faint-end slopes will lead to particularly stringent requirements on our understanding of the large-angle photometric variations in the survey. Regardless of the value of the faint-end slope, however, the bottom-right panel of Fig. 5 shows that the effects of the imperfectly estimated Galactic dust on the cosmological parameters can be very significant.

4.4 Example II: variability of survey depth

Our second example is based on the expectations of photometric depth variations of the Dark Energy survey. We use a map (Jim Annis, private communication) simulating observations over 525 night of observation spread over five years; see the top panel of Fig. 6. The observing conditions on the site are based on historical atmospheric data of the CTIO site between 2005 and 2010. The survey tiling strategy uses multiple massive overlaps to generate a survey that is as homogeneous as possible. Each part of the sky is imaged 10 times in each of the five DES filters (grizY). For simplicity, we only focus on the *i*-band survey-depth map.

The effect of the unaccounted-for variability in the survey depth is the same as that of the photometric calibration error. However, the variability is large and expected to be taken into account; therefore, we (arbitrarily) adopt the final calibration error to be equal to one-tenth of the depth-variation map (i.e. 1/10 of its amplitude shown in the top panel of Fig. 6). In other words, we assume

$$\text{calibration variations} \equiv \frac{1}{10} \times (i\text{-band variability map}).$$

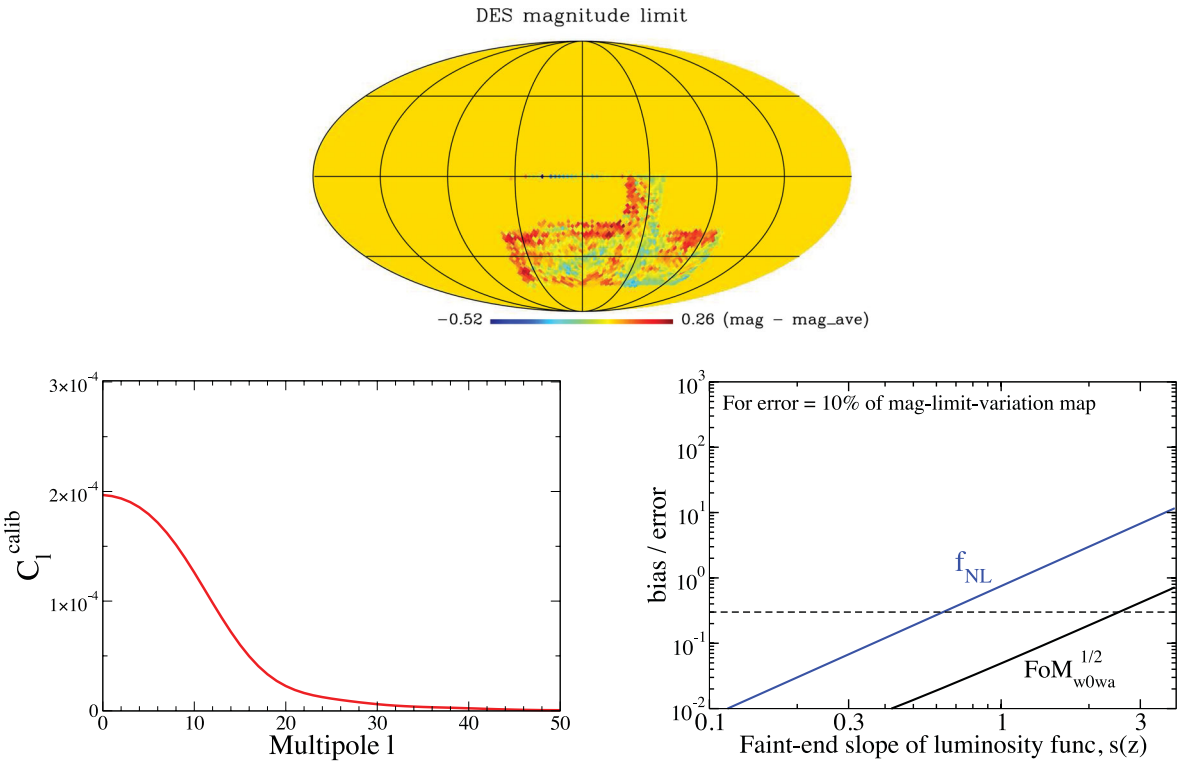

Figure 6. Top panel: *i*-band magnitude limits estimated for the upcoming observations of the Dark Energy Camera at CTIO as a function of angular position. The pattern of variations in the magnitude limits are set by the variations in the observing conditions and the survey tiling strategy over the five years of the survey. Bottom left: angular power spectrum of the magnitude limit map, extracted using POLSPICE and shown without the usual $\ell(\ell+1)/(2\pi)$ term so that the relative contribution of different multipoles can be more easily seen. Bottom right: biases in the cosmological parameters versus the faint-end slope of the luminosity function $s(z)$ assuming calibration error maps is consistent with a fixed *fraction* of 10 per cent of amplitude (or 1 per cent of power) of the magnitude-limit map shown in the top (bottom left) panel. The desired bias/error limit (horizontal dashed line) is exceeded for $s(z) \simeq 1$.

We follow the same procedure as with the dust example above, and calculate the power spectrum of the depth variability map using POLSPICE; see the bottom-left panel of Fig. 6. The variability of the survey depth will of course be accounted for in the data analysis – if it were not, it would lead to large biases in cosmological parameter estimates (as we easily verified using our formalism). The question is, then, to what accuracy do these variations need to be understood?

We answer that question by plotting, in the bottom-right panel of Fig. 6, the bias in the (square root of the) DE FoM, and non-Gaussianity parameter $f_{\rm NL}$, as a function of the faint-end slope of the luminosity function $s(z)$. As in the previous example of the corrections to the SFD dust maps, we find that the biases in the cosmological parameters are significant, and that they strongly depend on the faint-end slope of the luminosity function. In fact, even assuming that only 10 per cent of the variability in the survey depth is the 'calibration error' – the case shown in the bottom-right panel of the figure – the bias/error ratios are still large if $s(z) \gtrsim O(1)$.

5 CONCLUSIONS

In this paper, we made a first fully general study of the effect of the photometric calibration variations on the measured galaxy clustering angular power spectra. We derived a general formula for how a calibration variation with arbitrary spatial dependence affects the measured galaxy angular power spectrum. We illustrated the results assuming the standard set of cosmological parameters (including $f_{\rm NL}$), DES-type data set with five tomographic bins out to $z_{\rm max} = 1$, and two specific examples of real-world photometric calibrations. We now summarize our findings.

Photometric variations modulate the observed angular distribution of galaxy counts according to equation (2). This modulation translates into additive and multiplicative changes to the observed density fluctuation field, cf. equations (5) and (10), which in turn generate additive and multiplicative changes to the observed power spectrum.

As shown in equation (12), photometric variations across the survey masquerade as apparent violations of statistical isotropy. Hence, explicit tests of statistical isotropy could provide a useful way to identify unaccounted-for variations in the photometry. In this paper, we focused on the effects in the angle-averaged power-spectrum, cf. equation (15). We found that large-angle modulations of power (dipole, quadrupole, etc) are particularly damaging to cosmological analysis. We demonstrate this explicitly (cf. equation 28 and Fig. 2) for the case where the variance in the photometric calibration error field is concentrated in one multipole ℓ_1 at a time. Note that the spatially uniform photometric decrement or increment across the sky (i.e. the monopole, $\ell_1 = 0$) is unobservable since it only affects the mean number of galaxies in the survey.

Specializing in the angle-averaged power spectrum as done in equation (15), one can explicitly show that largest angle fluctuations are dominant (for a fixed induced variance on the calibration error field $c(\hat{\boldsymbol{n}})$); see Fig. 2. Moreover, the highest redshift clustering measurements are most susceptible to the photometric variations, essentially because their angular power is the smallest and is therefore most affected by the photometric variation.

Less obviously, we find that the additive errors (e.g. term proportional to $|c_{\ell m}|^2$ in equation 15) are typically dominant over the multiplicative biases (terms proportional to the coefficients U) for all redshift bins and at large angular scales. The reason is simple: because they couple different multipoles, multiplicative terms are suppressed relative to the additive ones by the fiducial angular power spectrum C_ℓ factor; see the term with C_{ℓ_2} in equation (15). Since $C_\ell \ll 1$ even at low z (and all ℓ), the additive terms dominate the error budget if all ℓ modes are used in the analysis. However, at slightly smaller angular scales ($\ell \gtrsim 10$), the multiplicative error terms dominate the error budget and can significantly bias the cosmological constraints, as discussed in Section 4. Therefore, it is important to include both multiplicative and additive aspects of the calibration error to accurately model biases in cosmological analyses.

The photometric variation calibration errors affect the galaxy clustering signal at large spatial scales, and lead to biases in the inferred cosmological parameters. Parameters describing dark energy and, especially, primordial non-Gaussianity are particularly affected since they imprint signatures in the clustering of galaxies precisely at these large scales. Figs 3 and 4, the principal plots in this paper, show these cosmological parameter biases for a fixed contribution of the calibration error at each multipole separately and for a range of multipoles, respectively. In Section 4, we further give two specific real-world examples of what the photometric variations could occur: errors in mapping the dust in our Galaxy, and variations in survey depth. We find that these calibration errors lead to potentially large cosmological biases, especially if the faint-end slope of the luminosity function $s = {\rm d}\log N/{\rm d}m|_{m_{\rm max}}$ is steep. In particular, in the Fisher matrix approximation, the cosmological parameter biases scale as s^2.

As a by-product of this work, we developed a reasonably fast algorithm, and provide a code[8], to calculate the full biased angular power spectrum of galaxies given an arbitrary photometric calibration variation map on the sky. As mentioned above, this calculation *would* be rather trivial if we could assume that the power spectrum errors are purely additive; however, we demonstrated that multiplicative errors are important and may in fact dominate, necessitating the more numerically intensive calculation for surveys of interest.

From our analyses, it appears that the total rms of the calibration error has to be kept at the level at somewhere between 0.001 and 0.01 mag, depending on how large a scale one wants to consider in order to maximize the extraction of cosmological information, in order not to bias the cosmological parameters appreciably. This is a very stringent requirement! Achieving it, however, may not be as difficult as it sounds given that this is the time-averaged error to be tolerated at the end of the whole survey. Moreover, there are several other tools that we have at our disposal that we did not consider in this preliminary work. For example, one could use the survey itself to internally determine

[8] www-personal.umich.edu/ huterer/CALIB_CODE/calib.html

('self-calibrate') the photometric variation errors, similarly to what weak lensing, cluster count, or Type Ia supernova surveys are doing or planning to do with their systematic errors. One could also use measurements of the higher point correlation functions to help determine these nuisance parameters (in our language, the $c_{\ell_1 m_1}$). We leave these promising avenues for future study.

ACKNOWLEDGEMENTS

We thank Jim Annis for providing the expectations of photometric depth variations for the DES, and Joshua Frieman, Enrique Gaztanaga, Andrew Hearin, Shirley Ho, Will Percival, Ashley Ross, Eddie Schlafly and Daniel Shafer for useful discussions. We also thank the anonymous referee for a number of useful suggestions. CC and DH are supported by the DOE OJI grant under contract DE-FG02-95ER40899. CC is also supported by a Kavli Fellowship at Stanford University. DH is additionally supported by NSF under contract AST-0807564, and NASA under contract NNX09AC89G. WF is supported by NASA under contract NNX12AC99G.

REFERENCES

Aihara H. et al., 2011, Astrophys. J. Suppl., 193, 29
Albrecht A. et al., 2006, preprint (arXiv:astro-ph/0609591)
Anderson L. et al., 2013, MNRAS, 428, 1036
Chon G., Challinor A., Prunet S., Hivon E., Szapudi I., 2004, MNRAS, 350, 914
Colless M. et al., 2001, MNRAS, 328, 1039
Copi C. J., Huterer D., Schwarz D. J., Starkman G. D., 2011, MNRAS, 418, 505
Dalal N., Dore O., Huterer D., Shirokov A., 2008, Phys. Rev., D, 77, 123514
Dawson K. S. et al., 2013, AJ, 145, 10
de Lapparent V., Geller M. J., Huchra J. P., 1986, ApJ, 302, L1
de Oliveira-Costa A., Tegmark M., 2006, Phys. Rev. D, 74, 023005
Drinkwater M. J. et al., 2010, MNRAS, 401, 1429
Efstathiou G., 2004, MNRAS, 349, 603
Gordon C., Hu W., Huterer D., Crawford T. M., 2005, Phys. Rev., D, 72, 103002
Hearin A. P., Gibelyou C., Zentner A. R., 2011, J. Cosmol. Astropart. Phys., 1110, 012
Heymans C. et al., 2006, MNRAS, 368, 1323
Ho S. et al., 2012, ApJ, 761, 14
Ho S., Hirata C., Padmanabhan N., Seljak U., Bahcall N., 2008, Phys. Rev. D, 78, 043519
Hoffman Y., Ribak E., 1992, ApJ, 384, 448
Hu W., Jain B., 2004, Phys. Rev. D, 70, 043009
Huterer D., Knox L., Nichol R. C., 2001, ApJ, 555, 547
Huterer D., Takada M., Bernstein G., Jain B., 2006, MNRAS, 366, 101
Huterer D., Turner M. S., 2001, Phys. Rev., D, 64, 123527
Jouvel S. et al., 2009, A&A, 504, 359
Kim J., Naselsky P., Mandolesi N., 2012, ApJ, 750, L9
Komatsu E. et al., 2011, Astrophys. J. Suppl., 192, 18
Mandelbaum R. et al., 2005, MNRAS, 361, 1287
Peek J., Graves G. J., 2010, ApJ, 719, 415
Ross A. J. et al., 2011, MNRAS, 417, 1350
Schlafly E. F., Finkbeiner D. P., 2011, ApJ, 737, 103
Schlegel D. J., Finkbeiner D. P., Davis M., 1998, ApJ, 500, 525
Scranton R. et al., 2002, ApJ, 579, 48
Smith R. E., Scoccimarro R., Sheth R. K., 2007, Phys. Rev. D, 75, 063512
Vogeley M. S., 1998, preprint (astro-ph/9805160)
York D. G. et al., 2000, AJ, 120, 1579
Zhan H., Knox L., Tyson J., 2009, ApJ, 690, 923

APPENDIX A: ANGULAR POWER SPECTRA AND THEIR INFORMATION CONTENT

We model the angular power spectra of galaxy density fluctuations as follows. In Limber's approximation, the angular power spectrum is given by

$$P_\ell^{(ij)} = \frac{2\pi^2}{\ell^3} \int_0^\infty \mathrm{d}z\, r(z) H(z) W_i(z) W_j(z) \Delta^2 \left(k = \frac{\ell}{r(z)}, z\right), \tag{A1}$$

where $\Delta^2(k) \equiv k^3 P(k)/(2\pi^2)$ is the dimensionless power spectrum, $r(z)$ is the comoving angular diameter distance and $H(z)$ is the Hubble parameter. The weights W_i are given by

$$W_i(z) = \frac{n(z)}{\int_{z_{\min}^{(i)}}^{z_{\max}^{(i)}} n(z)\mathrm{d}z} \left[H(z_{\max}^{(i)}) - H(z_{\min}^{(i)})\right], \tag{A2}$$

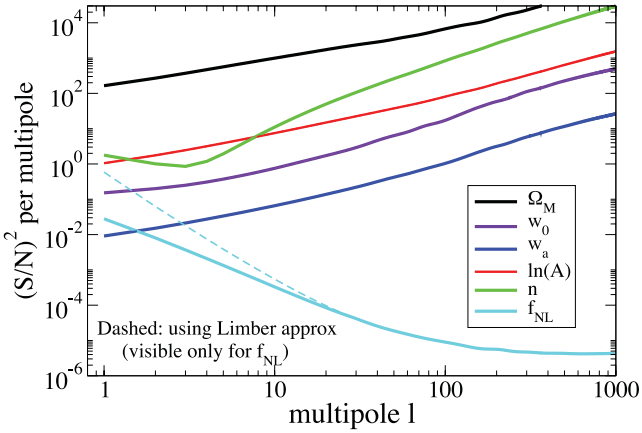

Figure A1. Signal-to-noise squared contribution (i.e. contribution to diagonal Fisher matrix element with no systematics present) per single multipole ℓ for each cosmological parameter. Note that we use the Limber approximation only at $\ell > 30$ in order to more accurately capture information on $f_{\rm NL}$ at $\ell \leq 30$.

where $H(x)$ is the Heaviside step function and $z^{(i)}_{\rm min}$ and $z^{(i)}_{\rm max}$ are the lower and upper bound of the ith redshift bin and $n(z)$ is the normalized radial distribution of galaxies[9] whose form we take to be

$$n(z) = \frac{1}{2z_0^3}\, z^2 {\rm e}^{-z/z_0}, \tag{A3}$$

which peaks at $z_{\rm max} = 2z_0$. In this work, we use $z_0 = 0.3$ so that the radial distribution peaks at redshift 0.6.

At the lowest multipoles, the Limber approximation is no longer accurate; see Fig. 1. At $\ell \leq 30$, we adopt the full expression for the power spectrum; using notation from e.g. Hearin, Gibelyou & Zentner (2011) this is

$$P_\ell^{(ij)} = 4\pi \int_0^\infty {\rm d}\ln k\, \Delta^2(k, z=0) I_i(k) I_j(k)$$
$$I_i(k) \equiv b_i(k) \int_0^\infty {\rm d}z\, W_i(z) \frac{D(z)}{D(0)}\, j_\ell(k\chi(z)), \tag{A4}$$

where $b_i(k)$ is the bias in ith redshift bin, $\chi(r)$ is the radial distance and $\chi(z) = r(z)$ in a flat universe that we consider. Here, $D(z)$ is the linear growth function of density fluctuations, so that $\delta(z) = [D(z)/D(0)]\delta(0)$. At multipoles $\ell > 30$, we continue to use the Limber approximation since the computation is much faster. The power spectra are shown in Fig. 1. Note that, when using equation (A4), the non-linear corrections to clustering are negligible since we only apply this equation at very large scales.

Fig. A1 shows the contribution to the signal-to-noise squared for each cosmological parameter separately per multipole – in other words, we show contribution to the Fisher matrix element F_{aa} for each parameter p_a from a single multipole ℓ. There is a clear trend of increased information at high multipoles, except for $f_{\rm NL}$ whose information largely comes at the lowest multipoles, despite cosmic variance (Dalal et al. 2008).

APPENDIX B: EXTRACTION OF FULL-SKY CALIBRATION FROM CUT-SKY DATA

In order to estimate the effect of photometric calibration errors, we perform all calculations in multipole space. In particular, our formalism requires the multipole coefficients of the calibration variation field, $c_{\ell_1 m_1}$, as input. In practice, this job will be left to observers who will have a number of tools at their disposal to estimate the photometric variation, as a function of sky position, in their survey. They or their theory colleagues, can then use our formalism, equation (15), to estimate the effect of calibration variations on the angular power spectra and the cosmological parameters.

However, it is non-trivial to obtain the coefficients $c_{\ell_1 m_1}$ given the cut-sky observations, i.e. partial sky coverage: recall, for example, that the Peek–Graves dust-correction map from Section 4.3 covers about 1/4 of the sky, while the DES depth map from Section 4.4 covers only 1/8 of the sky. Note that the naive reconstruction from the observed map, $c_{\ell_1 m_1} = \int Y^*_{\ell_1 m_1}(\hat{\boldsymbol{n}}) \delta N/N(\hat{\boldsymbol{n}}) {\rm d}\Omega$, would give the *cut-sky* multipoles which describe the field that is zero outside of the observed region, which we do *not* want: the cut-sky multipoles have wrong amplitudes and harmonic structure relative to the full-sky 'truth'.

Filling in the missing sky is a well-known problem in the CMB literature. While the reconstruction of the power C_ℓ is relatively straightforward, reconstruction of the temperature field $a_{\ell m}$ is challenging and typically works well only when substantial portions of the sky

[9] Note that a sometimes-used alternative definition of $n(z)$ refers to the spatial density of galaxies (e.g. Hu & Jain 2004); it is related to the quantity we use via ${\rm d}N/{\rm d}z = n(z)\, \Omega\, r^2(z)/H(z)$, where Ω is the solid angle spanned by the survey, and r and H are the comoving distance and Hubble parameter, respectively. Note also that our $W(z)$ is equivalent to the quantity $f(z)$ from Ho et al. (2008).

($f_{\rm sky} \gtrsim 0.8$) are observed. Fortunately, in this work we are only interested in obtaining *approximate* values for the $c_{\ell_1 m_1}$, consistent with the cut-sky map of the calibration field, in order to estimate its effects on cosmological parameters.

We have attempted, without success, two rather well-known techniques for reconstructing the true, full-sky $c_{\ell_1 m_1}$ from partial sky observations.

- We tried the direct reconstruction of the field, using the maximum-likelihood procedure (see e.g. Efstathiou 2004; de Oliveira-Costa & Tegmark 2006; Copi et al. 2011); this approach is used, for example, to reconstruct the CMB power at $\ell \lesssim 30$ (Komatsu et al. 2011). While this approach returns the true structure in the observed area of the sky (as it must), the reconstructions add spurious structure and extra power – clearly visible by eye – in the unobserved areas of the sky.
- We tried 'harmonic inpainting' (Hoffman & Ribak 1992; Kim, Naselsky & Mandolesi 2012) of our two maps, where the missing portion of the sky is filled in assuming that the density field is Gaussian, and starting with a guess for the covariance matrix of the field (which is given in terms of the theoretical angular power spectrum). As with the direct reconstruction, we find large spurious power in the unobserved portion of the sky in realistic cases when sky coverage is small, $f_{\rm sky} \ll 1$.

Given these failures and the fact that we only need a rough estimate of the full-sky calibration field $c_{\ell_1 m_1}$, we resort to the simpler scheme of reconstructing the large-angle power spectrum and drawing realizations of the field *consistent* with it. In particular, we

(i) calculate the angular power spectrum of the calibration field, $C_\ell^{\rm calib}$, from the cut-sky calibration map using POLSPICE package (Chon et al. 2004). POLSPICE uses the pixel-based approach to calculate the real-space angular power first and then, with appropriate apodizations, convert it to the $C_\ell^{\rm calib}$;

(ii) sample from this angular power spectrum, i.e. $c_{\ell_1 0} = \mathcal{N}(0, C_{\ell_1}^{\rm calib})$ and $c_{\ell_1 m_1}^{\rm Re,Im} = \mathcal{N}(0, C_{\ell_1}^{\rm calib}/2)$ for $m_1 \neq 0$, where $\mathcal{N}(\mu, \sigma^2)$ is the Gaussian normal function with mean μ and variance σ^2;

(iii) repeat the previous step a number of times to ensure appropriate averaging over realizations, though in practice we find that the each realization (for a fixed estimated $C_{\ell_1}^{\rm calib}$) leads to similar results.

The approach returned a smooth power spectrum at large scales (see the $C_\ell^{\rm calib}$ panels in Figs 5 and 6), and therefore reliable multipole coefficients describing calibration variations across the whole sky.

The reader might be worried that, in the above-mentioned successful approach, we assumed Gaussianity for the calibration field by assuming that the $C_{\ell_1}^{\rm calib}$ describes the full-sky field, and moreover assuming that the $c_{\ell_1 m_1}$ are Gaussian random variates. This is definitely an assumption needed to get the coefficients *in our particular examples* described in this Appendix but not in general. Moreover, we are not concerned about the assumption of Gaussianity of the calibration-variation field: equation (12), for example, illustrates that the calibration field will break statistical isotropy of the observed density fluctuations regardless of the nature of the statistical distribution of the ensemble from which th $c_{\ell_1 m_1}$ come from. Modest dispersion among the different m_1-modes in Fig. 3 confirms that the principal property of these coefficients that drives their effect on cosmology are their amplitudes as a function of ℓ_1, not their phases.

We emphasize here that the somewhat-challenging task of needing to determine the (full-sky) $c_{\ell_1 m_1}$ discussed in this Appendix is largely orthogonal to the overall goal of this paper of quantifying the effects of photometric variations. In practice, the observers will have an opportunity to estimate the photometric calibration variations across the sky in real space using a number of methods (e.g. using theoretical estimates, or measurements across part of the sky as we did in our examples). Converting from $c(\hat{\boldsymbol{n}})$ to the full-sky $c_{\ell_1 m_1}$ is then just a purely mathematical exercise in which only an approximate answer is required.

APPENDIX C: TABULATION OF COEFFICIENTS

In order to speed up the calculations of the observed galaxy overdensity field $t_{\ell m}$ and its correlations in harmonic space, we need to calculate a very large number of geometrical quantities $R^{\ell_1 \ell_2 \ell}_{m_1 m_2 m}$; see equations (11)–(13). Recall that each (ℓ, m) pair has $2\ell + 1$ quantities for a fixed ℓ, or approximately $\ell_{\rm max}^2$ quantities for all ℓ up to some $\ell_{\rm max}$. Calculating all of the R coefficients would then naively involve $O(\ell_{\rm max}^6)$ operations which, for $\ell_{\rm max} \simeq 1000$, would be 10^{18} calculations of the Wigner-3j symbols! Calculating even a fraction of such a large number of coefficients is clearly unfeasible.

We bring the computation required to a manageable size and speed as follows. We decide to tabulate the coefficients U for the minimum required number of quadruplets of its indices, and carry out the summation in equation (13) for each U. Moreover, since our goal is to concentrate on the large-angle (low-ℓ_1) systematics, which limits the maximum multipole *of the systematics*, ℓ_1 (see equation 13), we choose $\ell_1 \leq \ell_{\rm calib,max}$ with $\ell_{\rm calib,max} = 20$. Therefore, the total number of evaluations of the Wigner-3j symbols will be approximately equal to the number of (ℓ_1, m_1) pairs times the number of the U coefficients; the former quantity is

$$N_{\ell_1, m_1} = \sum_{\ell_1 = 0}^{\ell_{\rm calib,max}} (2\ell_1 + 1) = (\ell_{\rm calib,max} + 1)^2, \tag{C1}$$

while the latter quantity we now evaluate.

At a fixed multipole of the *true* density field ℓ_2 and a calibration error at some multipole ℓ_1, only the *observed* multipoles in the range $\max\{(\ell_2 - \ell_1), 0\} \leq \ell \leq \ell_2 + \ell_1$ are affected; this is a well-known feature of the coupling of angular momenta in e.g. quantum mechanics. Therefore, for fixed values of ℓ and m, the total number of (ℓ_2, m_2) pairs that can possibly lead to non-zero U coefficients is naively

$N_{\ell_2,m_2} = \sum_{\ell-\ell_{\rm calib,max}}^{\ell+\ell_{\rm calib,max}}(2\ell_2+1)$. However, we must also remember of a selection rule[10] that $m_1 + m_2 = m$, which means that for a fixed observed-field coefficient m and calibration-field coefficient m_1, only *one* coefficient m_2 (instead of $2\ell_2 + 1$ of them) survives. Therefore, for a fixed ℓ, the *total* number of U coefficients to tabulate (e.g. for use in equation 15) is of the order of

$$N_{m,\ell_2,m_2,\ell_1,m_1} \simeq (2\ell+1)(2\ell_{\rm calib,max}+1)N_{\ell_1,m_1} \simeq 4\,\ell\,\ell^3_{\rm calib,max}, \tag{C2}$$

where the factors of $2\ell + 1$ and $2\ell_{\rm calib,max} + 1$ refer to the number of m coefficients and (ℓ_2, m_2) pairs, respectively. So for a typical calculation with $\ell_{\rm calib,max} \simeq 20$, the number of evaluations for a single multipole $\ell \sim 250$ is of the order of 10^7; for of the order of 30 values of ℓ, including the densely spaced coverage of the lowest observable multipoles where the effects of photometric variation are the largest, this is still less than $O(10^9)$ evaluations of the Wigner-3j symbols, which is entirely feasible and takes of the order of a minute on a single 16-core desktop computer.

The last detail is an actual computation of the Wigner-3j symbols: we use the `Gnu Scientific Library` (GSL) routines at $\ell \leq 50$. At higher multipoles these break down, and we use a special purpose routine[11] that uses approximate expressions for the Wigner coefficients. These more accurate expressions hold provided $\ell, \ell_2 \gg \ell_1$, but given that $\ell > 50$ in the regime we are using this approximation and the fact that the multipole that corresponds to the calibration error is no bigger than $\ell_1 \leq \ell_{\rm calib,max} = 20$, this condition always holds.

[10] The full list of selection rules for non-zero Wigner-3j symbols is $\max[|\ell_i - \ell_j|, 0] \leq \ell_k \leq \ell_i + \ell_j$ and $|m_i| \leq \ell_i$ where $\{i, j, k\}$ correspond to the permutations of subscripts 1, 2, and no subscript. Moreover, $m_1 + m_2 + m = 0$, and when $m_1 = m_2 = m = 0$ then $\ell_1 + \ell_2 + \ell$ must be even.
[11] http://www.gnu.org/software/gsl/.

This paper has been typeset from a TEX/LATEX file prepared by the author.